Supporting Information for

SiC-C Composite as A Highly Stable and Easily Regenerable Photothermal Material for Practical Water Evaporation

Le Shi, Yusuf Shi, Renyuan Li, Jian Chang, Noor Zaouri, Elaf Ahmed, Yong Jin, Chenlin Zhang, Sifei Zhuo and Peng Wang*
Water Desalination and Reuse Center, Division of Biological and Environmental Sciences and Engineering, King Abdullah University of Science and Technology, Thuwal 23955-6900, Saudi Arabia. E-mail: peng.wang@kaust.edu.sa

Contents of the Supporting Information

Total number of pages: 21

Total number of figures: 22

Total number of tables: 3

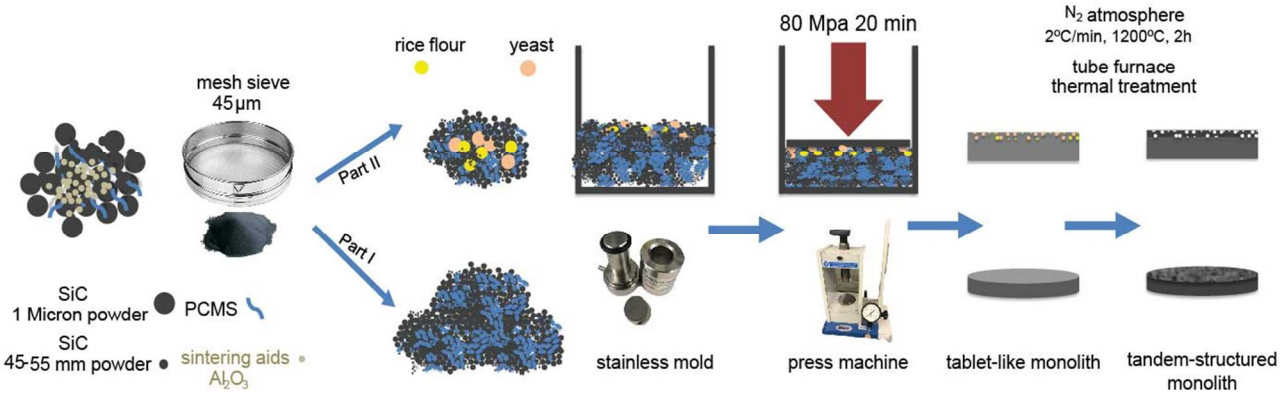

Figure S1 Synthesis process of tandem-structured SiC-C monoliths.

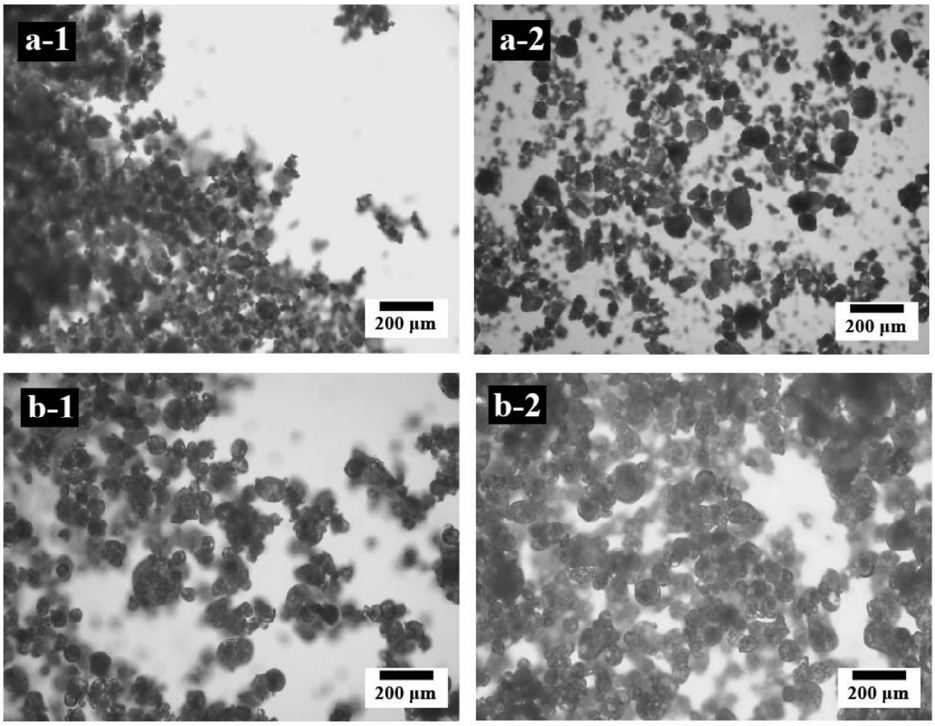

Figure S2 Mircoscopic images of yeast and rice flour powder (5X). a-1 and a-2 are the rice flour powder in dry and wet conditions. b-1 and b-2 are the yeast in dry and wet conditions. The wet condition is created by soaking the powders in tolune solvent.

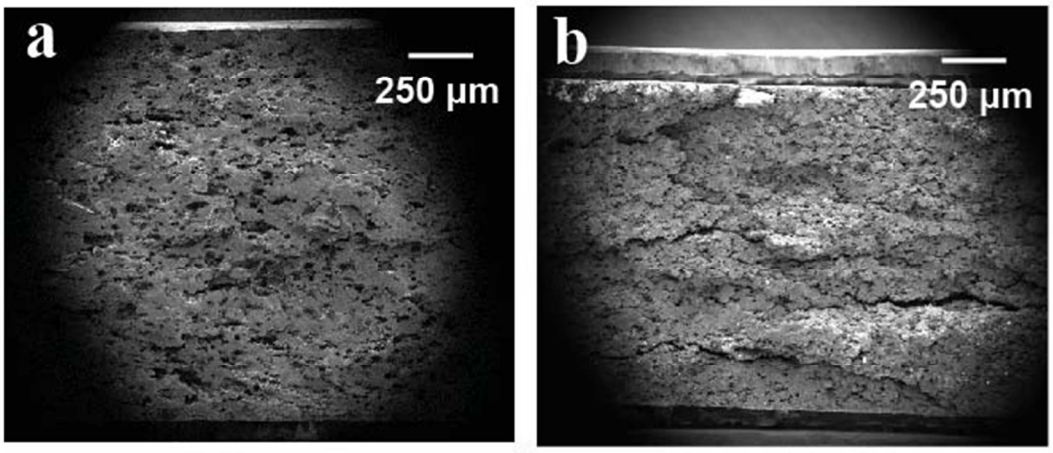

Figure S3 SEM images of cross section of single layer porous SiC-C (0.09y +0.09r) monolith with yeast and rice flour as sacrificial templates (a) and single layer porous SiC-C (0.18y) monolith with yeast as sacrificial templates.

Two different sacrificial templates are used in order to produce different sizes of pores, and the sizes of yeast and rice flour are presented in Figure S2. In comparison, a single layered porous SiC-C monolith with only yeast as a sacrificial template is prepared (Figure S3b), with the same mass ratio of sacrificial templates used in Figure 2b. It is clear to see from Figure S3b that the sample prepared with yeast and rice flour has a much compact structural support, while the sample prepared with only yeast has a lot of visible cracks inside the monolith, which are unfavorable for a highly mechanical stable material.

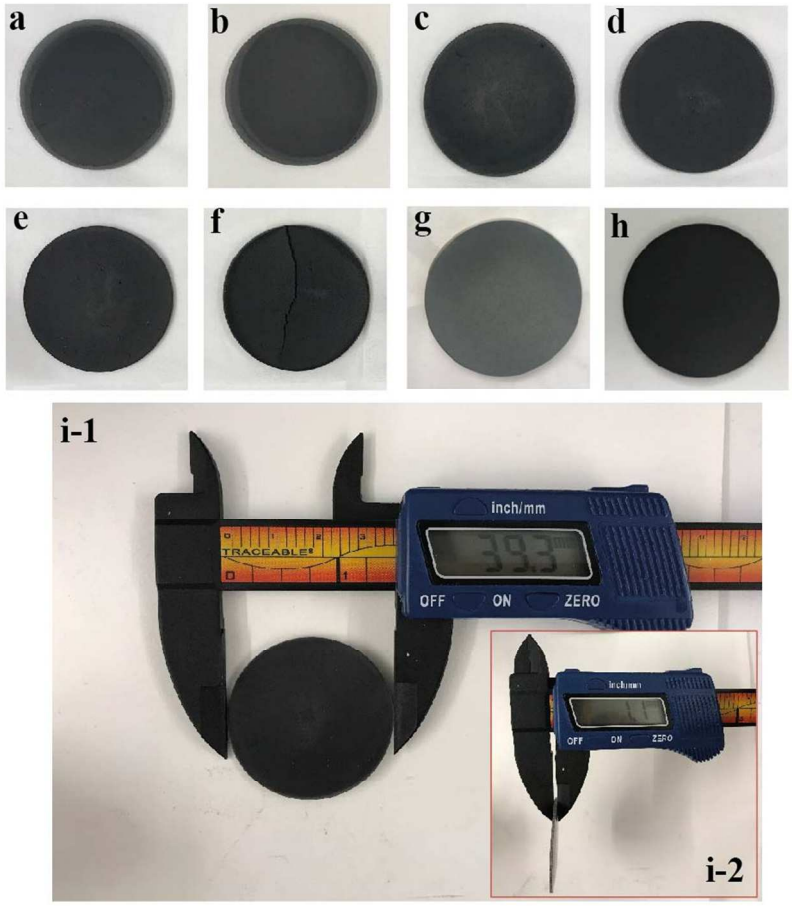

Figure S4 Digital photos of SiC-C dense monolith without Al_2O_3 (a), SiC-C dense monolith (b), SiC-C (0.03y +0.03r) monolith (c), SiC-C (0.06y +0.06r) monolith (d), SiC-C (0.09y +0.09r) monolith (e), SiC-C (0.12y +0.12r) monolith (f), SiC-C (0.09y +0.09r) monolith before annealing treatment (g), and SiC-C (0.09y +0.09r) porous monolith (h). Diameter and thickness of SiC-C (0.09y +0.09r) monolith (i).

For a comparison, the single layer dense SiC-C monolith without Al_2O_3, tandem-structured SiC-C composite monolith before annealing and single layer porous SiC-C composite monolith are also presented. It is observed that the visual color of the samples is darker as the amounts of sacrificial templates increase. However, there is no visible cracks in the materials until the quantities of the sacrificial templates is increased to be 0.12 g yeast and 0.12 g rice flour (Figure S2-f). The annealed sample shows darker color than the same sample before annealing (Figure S2-g), which means the free carbon content in the monolith is increased by the annealing treatment.

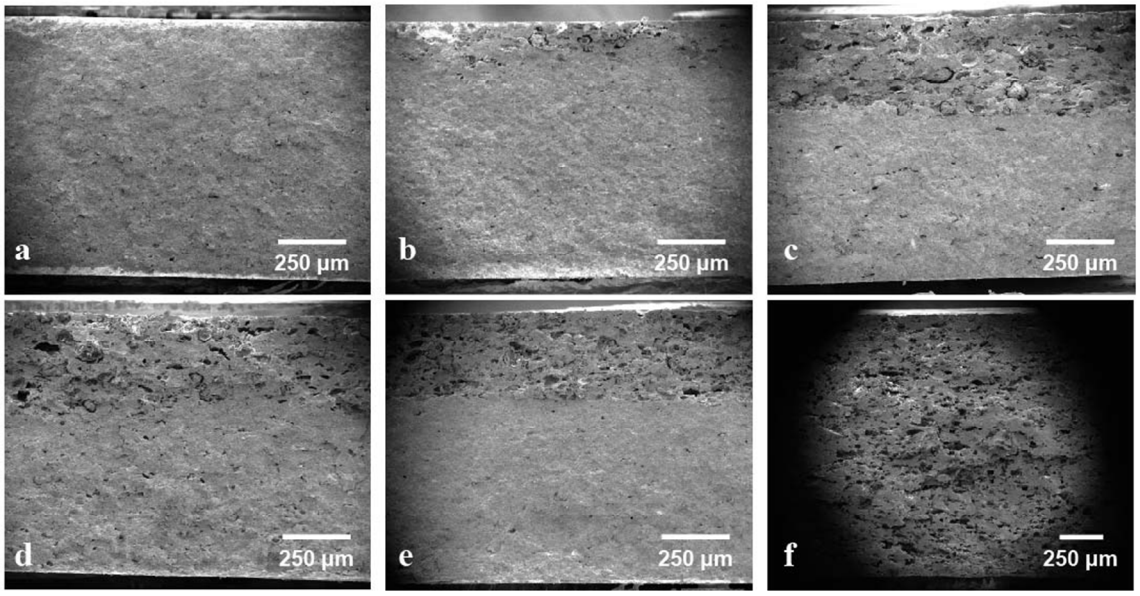

Figure S5 SEM images of cross section of SiC-C dense monolith (a), SiC-C (0.03y +0.03r) monolith (b), SiC-C (0.06y +0.06r) monolith (c), SiC-C (0.09y +0.09r) monolith (d), SiC-C (0.12y +0.12r) monolith (e) and SiC-C (0.09y +0.09r) porous monolith with yeast and rice flour as sacrificial templates (f).

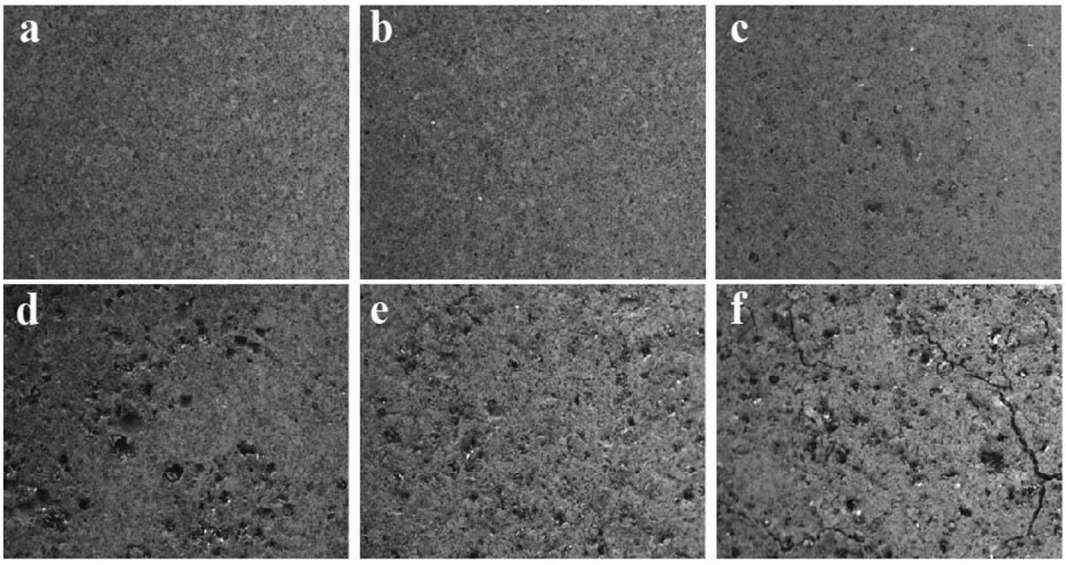

Figure S6 Top view microscopic images (5X) of SiC-C dense composite monolith without Al_2O_3(a), SiC-C dense monolith (b), SiC-C (0.03y +0.03r) monolith (c), SiC-C (0.06y +0.06r) monolith (d), SiC-C (0.09y +0.09r) monolith (e), SiC-C (0.12y +0.12r) monolith (f).

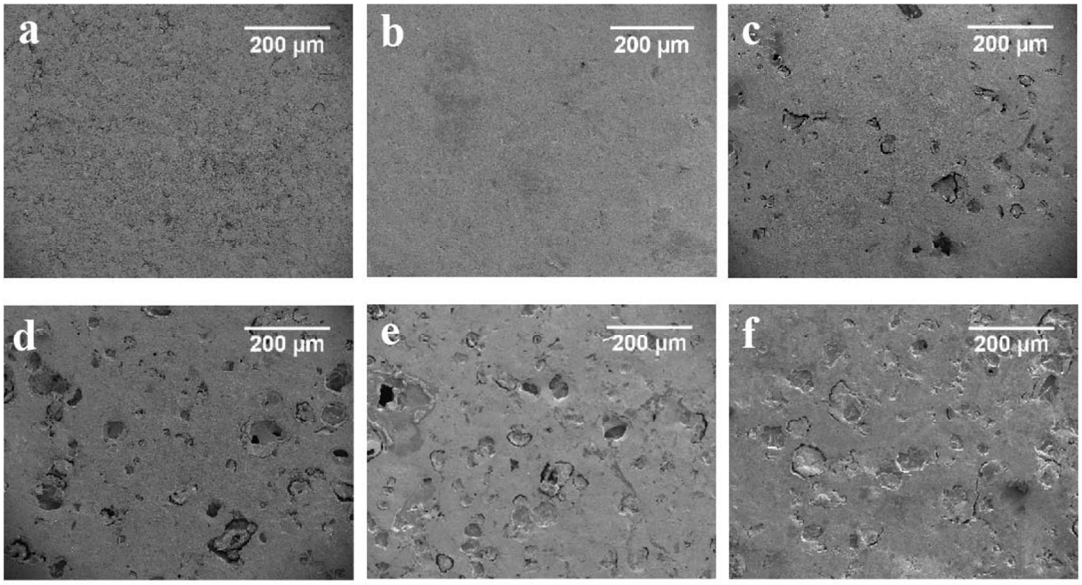

Figure S7 Top view SEM images of SiC-C dense monolith without Al_2O_3 (a), SiC-C dense monolith (b), SiC-C (0.03y +0.03r) monolith (c), SiC-C (0.06y +0.06r) monolith (d), SiC-C (0.09y +0.09r) monolith (e), SiC-C (0.12y +0.12r) monolith (f).

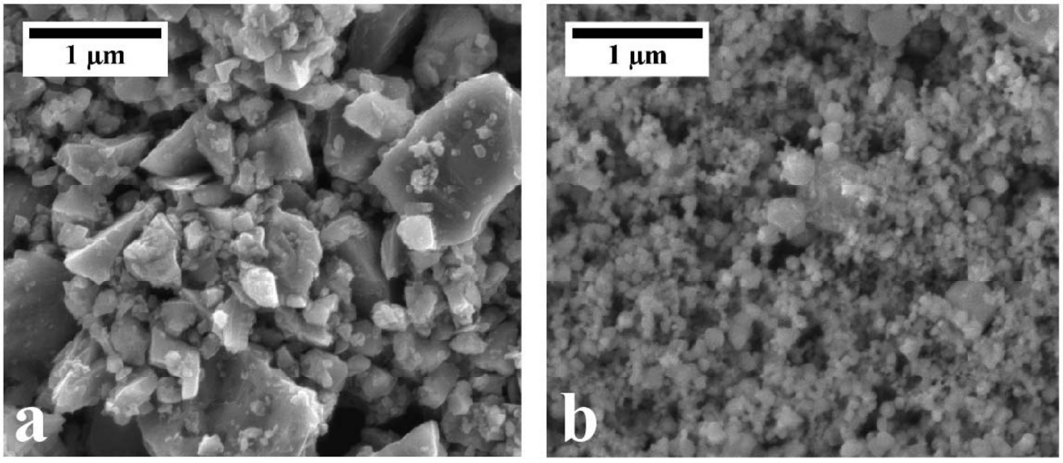

Figure S8 SEM images of two different SiC precursor powders: (a) big SiC particle, micron powder, 14-19 $m^2 g^{-1}$, (b) small SiC particle, nano powder, 44-45 nm, 70-90 $m^2 g^{-1}$.

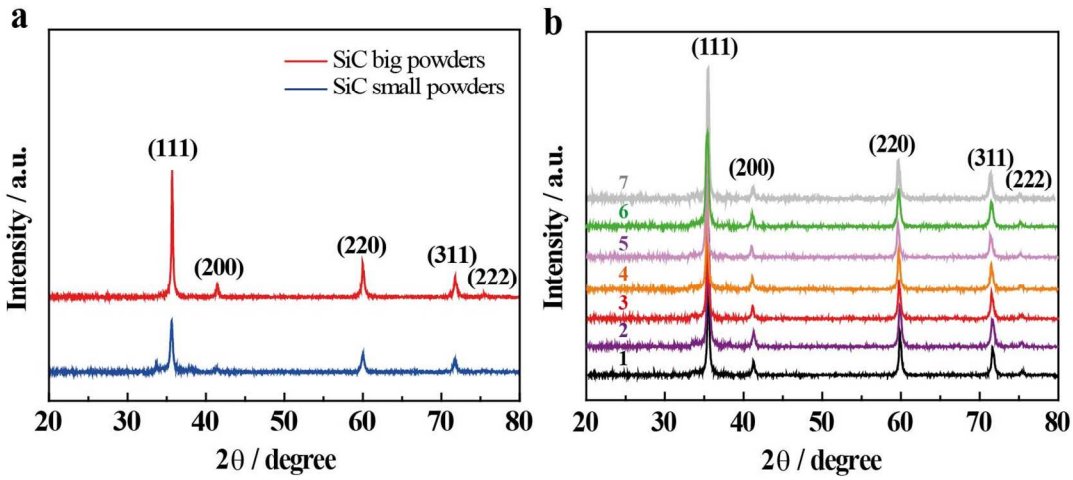

Figure S9 XRD spectra of SiC-C monolith before annealing treatment and after annealing treatment: (a) two different SiC precursor powders, and (b) SiC-C dense monolith without Al_2O_3 (b-1), SiC-C dense monolith (b-2), SiC-C porous monolith (b-7) and tandem-structured SiC-C composite monolith with different amount of sacrificial templates: 0.03y +0.03r (b-3), 0.06y +0.06r (b-4), 0.09y +0.09r (b-5) and 0.12y +0.12r (b-6).

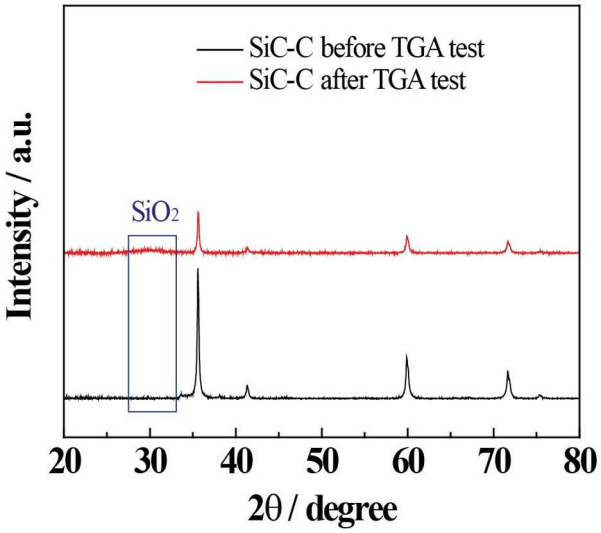

Figure S10 XRD spectra of SiC-C (0.09y +0.09r) monolith residues after TGA analysis.

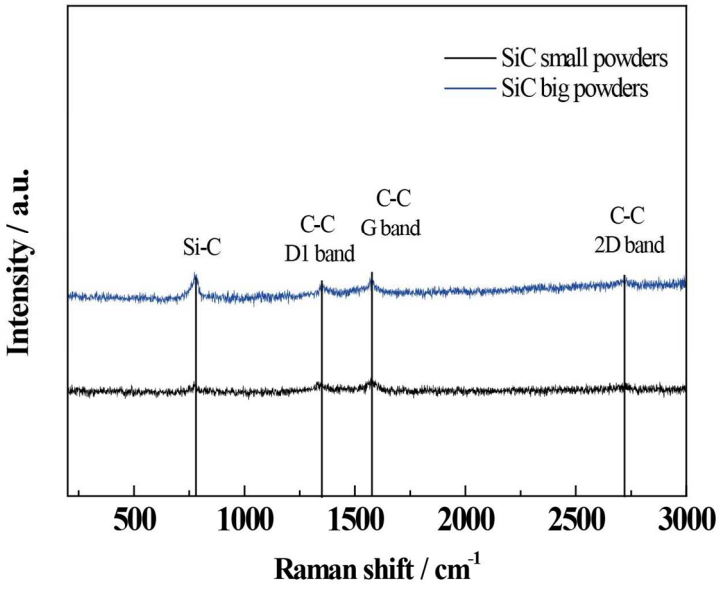

Figure S11 Raman spectra of SiC precursor powders in big size and small size. Raman spectra measured with 473 nm laser wavelength excitation.

Typical bands from C-C are observed in SiC precursor powders, which means that there is by-product carbon in the commercial SiC powders.

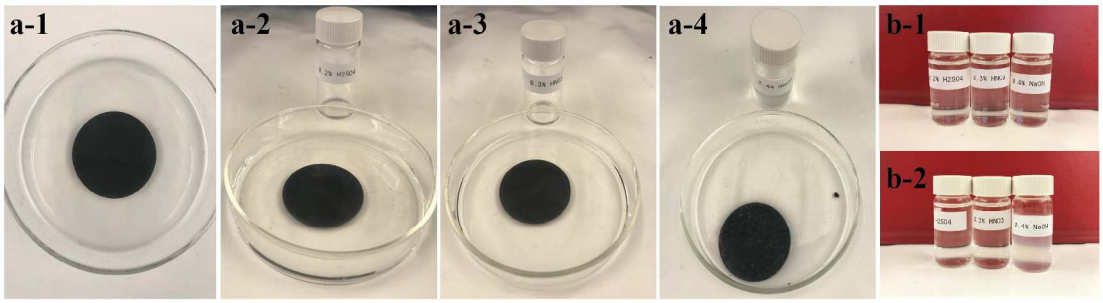

Figure S12 Freshly prepared SiC-C monolith sample (a-1), SiC-C monolith sample immersed in 0.2% H_2SO_4 (a-2), 0.3% HNO_3 (a-3), and 0.4% NaOH (a-4), for 10 min respectively. Chemical agents (0.2% H_2SO_4, 0.3% HNO_3 and 0.4% NaOH) before (b-1) and after (b-2) the SiC-C monolith cleaning.

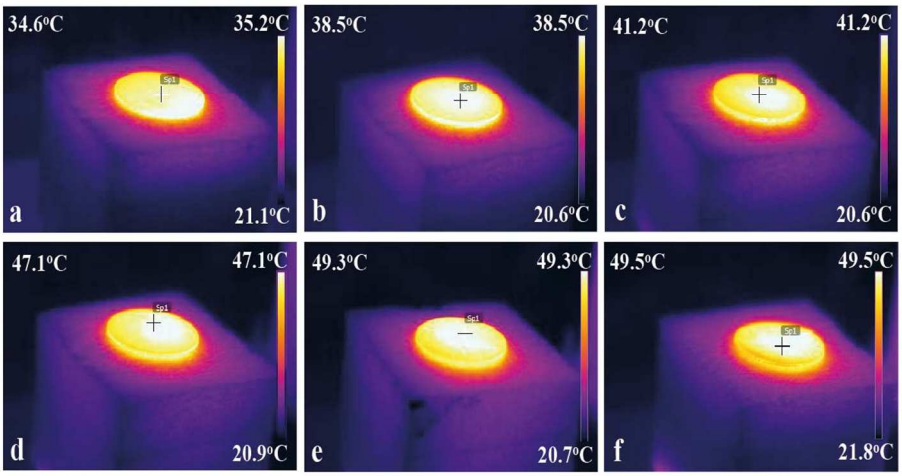

Figure S13 IR images of tandem-structured SiC-C monolith samples under illumination for 60 s: SiC-C dense monolith without Al_2O_3 (a), SiC-C dense monolith (b), SiC-C (0.03y +0.03r) monolith (c), SiC-C (0.06y +0.06r) monolith (d), SiC-C (0.09y +0.09r) monolith (e), SiC-C (0.12y +0.12r) monolith (f).

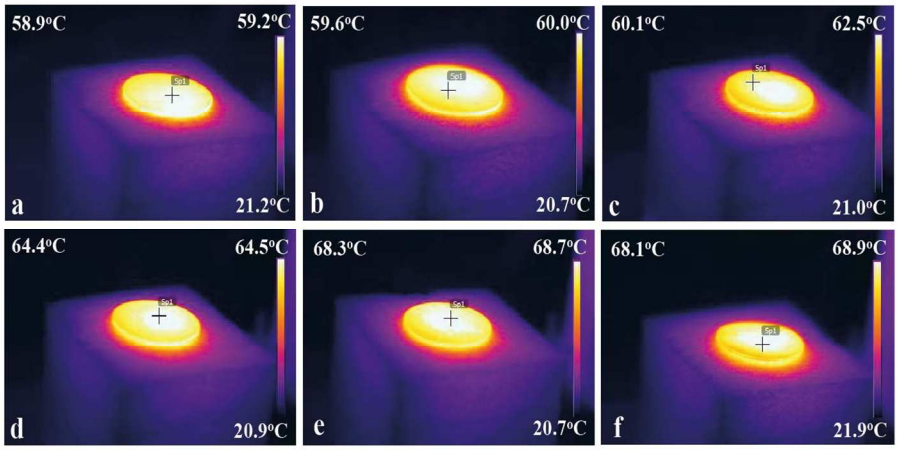

Figure S14 IR images of tandem-structured SiC-C monoliths under illumination for 900 s: SiC-C dense monolith without Al_2O_3 (a), SiC-C dense monolith (b), SiC-C (0.03y +0.03r) monolith (c), SiC-C (0.06y +0.06r) monolith (d), SiC-C (0.09y +0.09r) monolith (e), SiC-C (0.12y +0.12r) monolith (f).

The light to evaporation conversion efficiency (η) of all the samples are calculated using the following equation (1):

$$\eta = \frac{Q_e}{Q_s} \qquad (1)$$

where Q_s is the power density of solar illumination (1000 Wm^{-2}) and Q_e is the power needed for water evaporation, which is calculated using the following equation (2):

$$Q = \frac{dm \times H_e}{dt} = \upsilon \times H_e \qquad (2)$$

where *m* is the mass of the evaporated water, *t* is the evaporation time, H_e is the heat of water evaporation ($\approx$ 2270 kJ kg^{-1}) and υ is the water evaporation rate, which is calculated by using the following equation (3):

$$\upsilon = \frac{dm}{S \times dt} \qquad (3)$$

where *m* is the mass of the evaporated water, *S* is the surface area of the SiC-C monolith, and *t* is the duration time.

The dynamics of η as a function of illumination time for DI water evaporation and synthetic seawater evaporation are presented in Figure S14 and Figure S15. It is important to mention here that the surface area used for calculation is 12.13 cm^2 with a monolith diameter of 3.93 mm. The water pump provided by two orthometric strips of cotton cloth on the surface of the SiC-C monolith supposedly affects the light absorption, which means the effective surface area for water evaporation is smaller than 12.13 cm^2. As a result, the calculation results obtained here for water evaporation rate and water evaporation efficiency are supposedly smaller than the actual value of evaporation rate and efficiency.

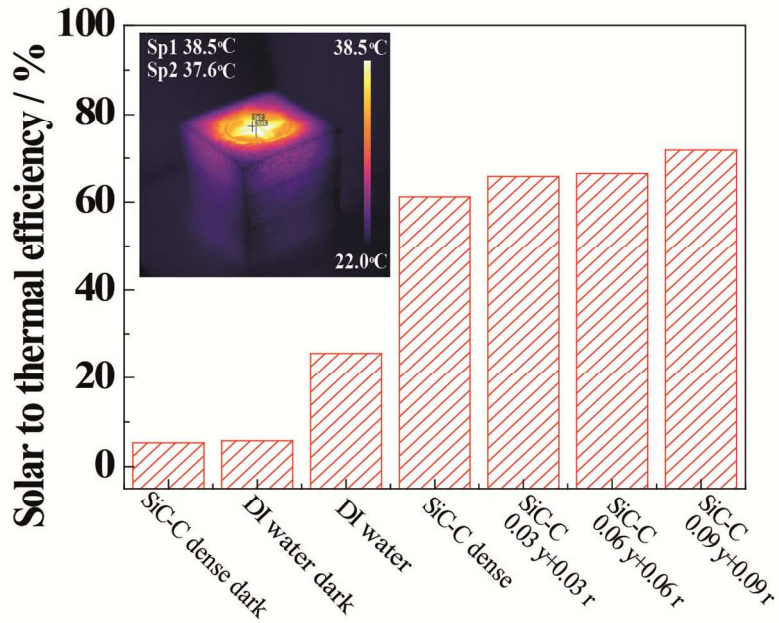

Figure S15 The average DI water evaporation efficiency of final 30 minutes by SiC-C monoliths. The inset shows the surface temperature of SiC-C (0.09y+0.09r) monolith during evaporation.

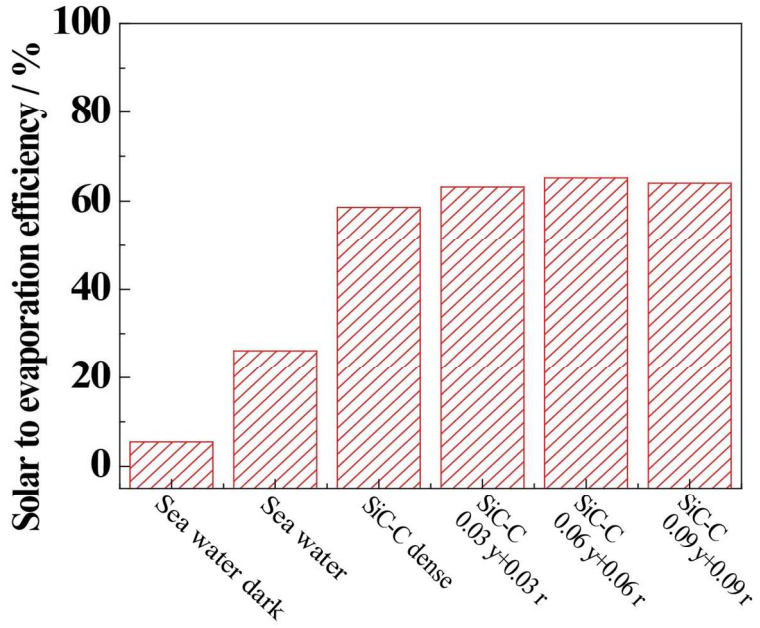

Figure S16 The average synthetic seawater evaporation efficiency of final 30 minutes by SiC-C monoliths. (3.5% NaCl)

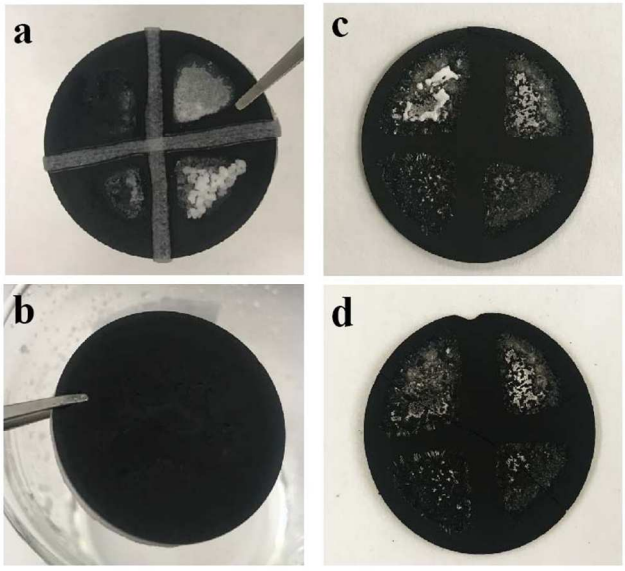

Figure S17 Images of SiC-C (0.09y+0.09r) monolith with salts precipitation from 3.5% NaCl solution (a) and after water flushing cleaning (b); salts precipitation from during the evaporation of the commercial synthetic seawater (c) and after water flushing cleaning (d).

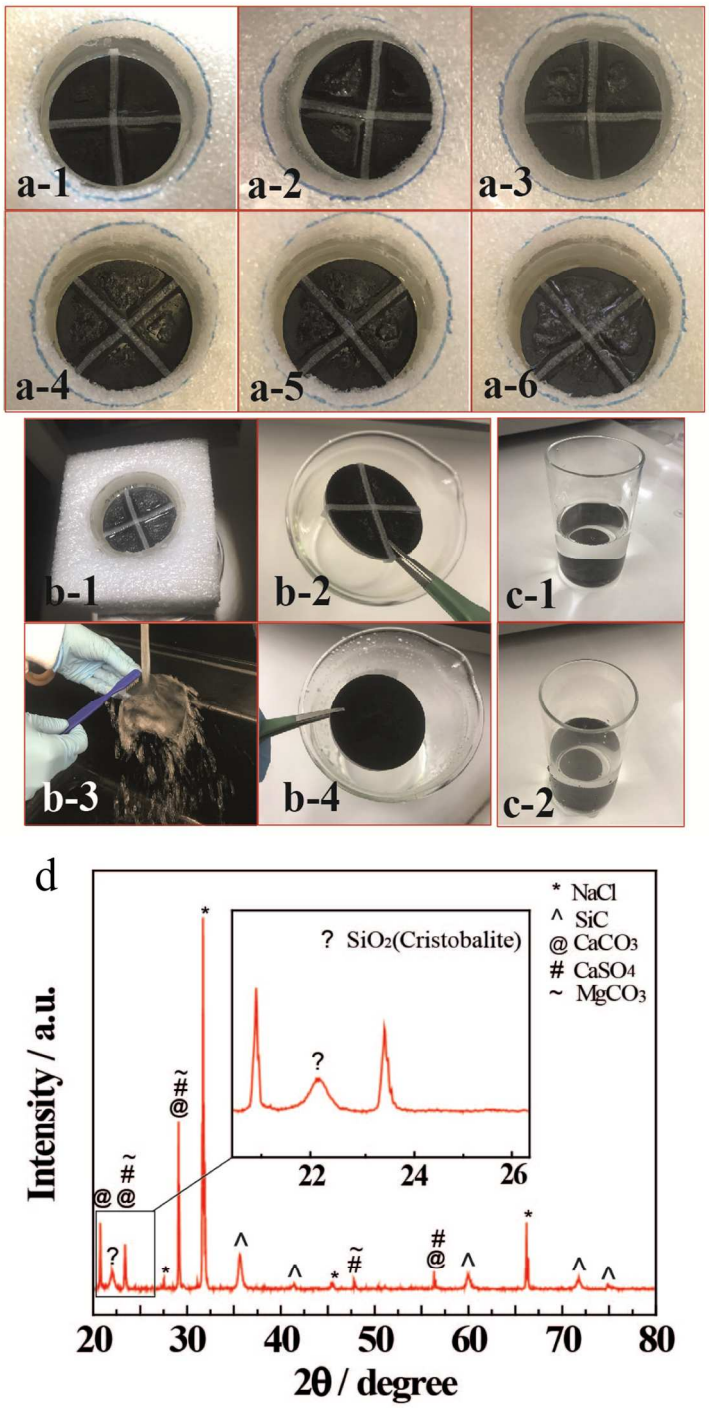

Figure S18 The digital photos (a-1 to a-6) present the fouling layer growing after each cycle. The digital photos (b-1 to b-4) present the fouling layer cleaning after each cycle with water flushing and brushing under tap water. The digital photos c-1 and c-2 present the water beaker with SiC-C monolith before sonication and after sonication cleaning process. (d) High resolution XRD results for the salts precipitation on the surface of SiC-C monolith after water evaporation by using Red Sea water.

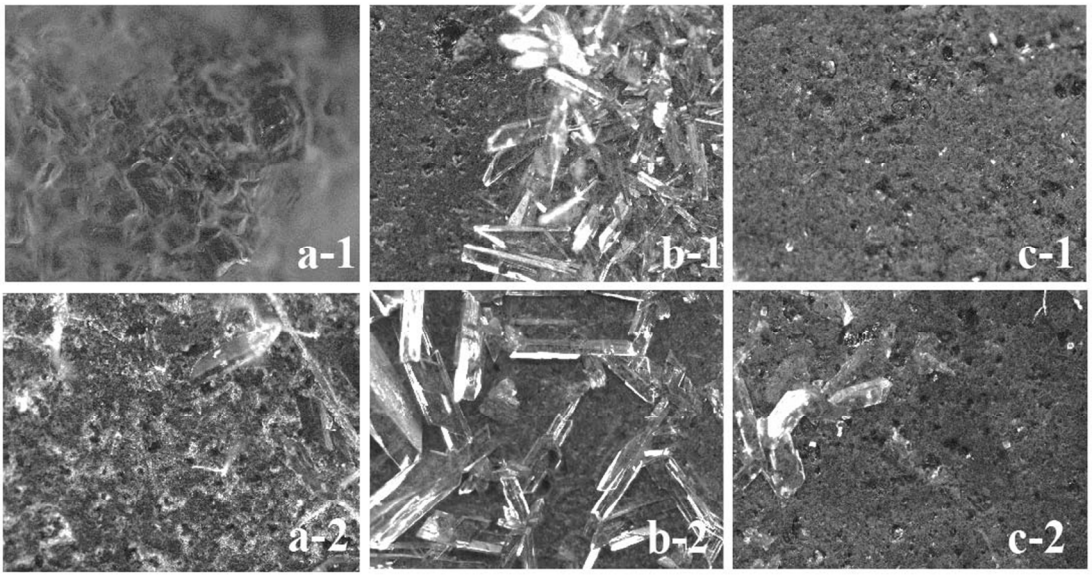

Figure S19 Top view microscopic images of SiC-C (0.09y+0.09r) monolith under different conditions: after water evaporation in raw Red Sea water for 6 cycles (a), after physical fouling cleaning by flushing DI water (b), and after physical fouling cleaning with brush (c).

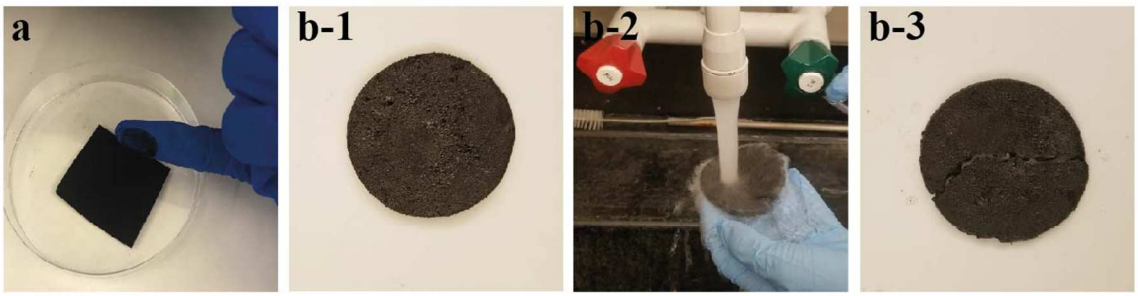

Figure S20 comparison of mechanical structure stability between different photothermal materials: (a) carbon black deposited on the support of AAO membrane, (b) rGO foam prepared by ice-dried method, (c) rGO foam cleaning under water flushing, and (d) rGO foam is broken after water flushing.

As for comparison, another two samples prepared in different way following the previous literatures are presented in Figure S12. One experiment involved depositing a carbon layer on an AAO membrane via a common vacuum filtration method[4](Figure S12a). The carbon black in this case could easily come off the AAO support layer. The other experiment involved preparing a rGO sponge by freeze-drying[46] and it turned out that the rGO sponge was very fragile and was not able to undergo a flow-water washing process (Figure S12b).

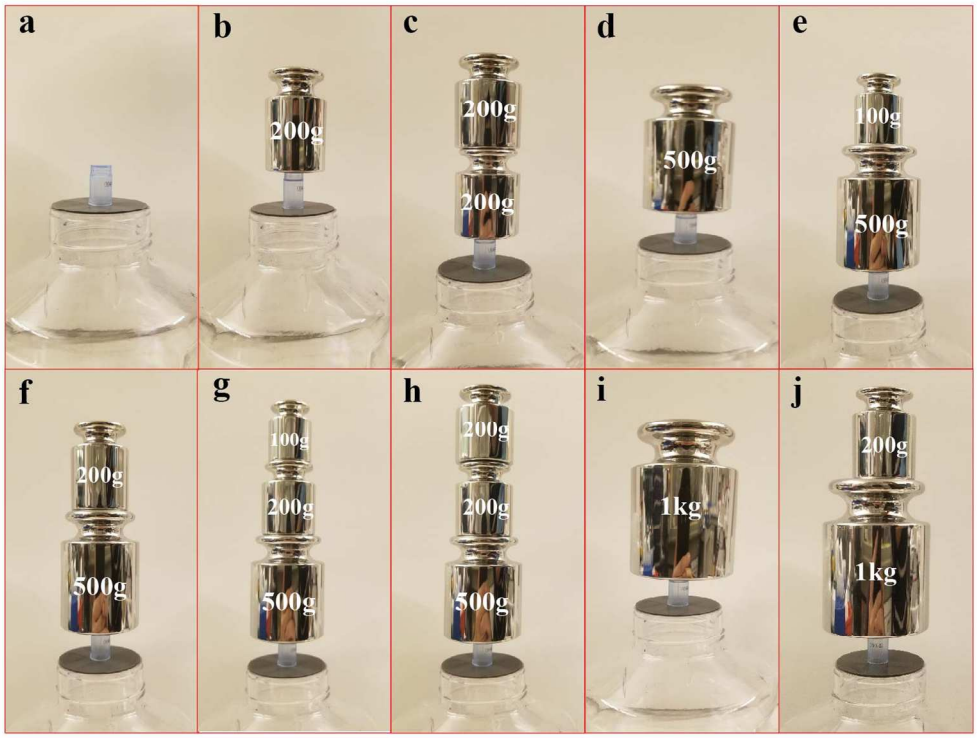

Figure S21 Pressure test for the SiC-C (0.09y+0.09r) monolith sample (the pressure is calculated as p=mg/A, where p is pressure, m is weight, A is contact area): (a) with a column (contact area of 13.98 mm^2); (b) with a weight of 200 g (0.14×10^6 Pa); (c) with a weight of 400 g (0.28×10^6 Pa); (d) with a weight of 500 g (0.35×10^6 Pa); (e) with a weight of 600 g (0.42×10^6 Pa); (f) with a weight of 700 g (0.49×10^6 Pa); (g) with a weight of 800 g (0.56×10^6 Pa); (h) with a weight of 900 g (0.63×10^6 Pa); (i) with a weight of 1 kg (0.7×10^6 Pa); and (j) with a weight of 1.2 kg (0.84×10^6 Pa).

In order to further confirm the mechanical strength of the SiC-C monolith in this work, additional test was conducted. A sample of the tandem-structured SiC-C monolith was directly put onto the mouth of a bottle, whose mouth's outer diameter is exactly same as the diameter of SiC-C monolith (Figure S21). Then a series of weights were put on the center of the SiC-C monolith sample to test the biggest pressure it could hold. Since the pressure is evaluated by the force applied perpendicular to the surface of an object per unit area over which that force is distributed, all the weights are put on a same column (with an inner diameter of 8.4 mm and outer diameter of 9.4 mm) to keep a same contact area (13.98 mm^2) between the weight and the surface of SiC-C monolith sample. Then the increase of the pressure is simplified by increasing the weight on the surface of SiC-C monolith sample. It turns out that the SiC-C monolith sample was able to withstand a relatively big pressure as high as 0.84×10^6 Pa.

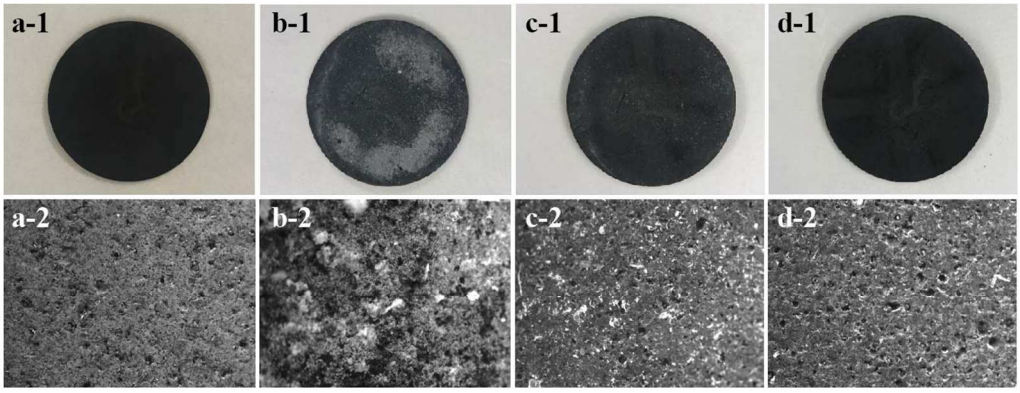

Figure S22 Top view digital photos and microscopic pictures (5X) of SiC-C (0.09y+0.09r) monolith under different conditions with wastewater 2 (secondary treated wastewater, after the aerobic MBR from WWTP in KAUST): the freshly prepared SiC-C (0.09y+0.09r) monolith (a-1 and a-2), SiC-C (0.09y+0.09r) monolith with fouling layers after water evaporation in wastewater (b-1 and b-2), SiC-C (0.09y+0.09r) monolith with fouling layers after cleaning with water flushing (c-1 and c-2), and SiC-C (0.09y+0.09r) monolith with fouling layers after cleaning with brushing (d-1 and d-2).

The WWTP is equipped with the following process units: (i) a grid mesh screen to remove bulky items in the incoming wastewater stream, (ii) a primary clarifier, (iii) an anoxic-oxic activated sludge tank, (iv) an aerobic membrane bioreactor (MBR), and (v) a holding tank for chlorination. Five liters of effluent was collected after the aerobic MBR, which is used for the water evaporation test with our SiC-C (0.09y+0.09r) monolith.

Table S1 Ion composition of commercial synthetic seawater.

Species	Formula	Concentration
Sodium Chloride	NaCl	24.52 g/L
Magnesium Chloride	$MgCl_2$	5.20 g/L
Sodium Sulfate	Na_2SO_4	4.09 g/L
Calcium Chloride	$CaCl_2$	1.16 g/L
Potassium Chloride	KCl	0.695 g/L
Sodium Bicarbonate	$NaHCO_3$	0.201 g/L
Potassium Bromide	KBr	0.101 g/L
Boric Acid	H_3BO_3	0.027 g/L
Strontium chloride	$SrCl_2$	0.0025 g/L
Sodium Fluoride	NaF	0.003 g/L
Water	H_2O	988.969 g/L
Total		1025g/L

Table S2. Ion composition of seawater (Red Sea).

Ion composition	Cl^-	Na^+	SO_4^{2-}	Mg^{2+}	Ca^{2+}	K^+	HCO_3^-	Br^-	Total dissolved solids (TDS)
Concentration (g/L)	22.219	14.255	3.078	0.742	0.255	0.210	0.146	0.072	41.000

Table S3. Water quality test of different water samples.

Parameter	DI water	NaCl (3.5%)	Seawater Red Sea	Wastewater 1	Wastewater 2
DOC (mg/l)	< 5µg/l	< 5µg/l	1.272	93.28	2.34
pH	6.04	4.95	8.20	7.24	6.80

Langelier Saturation Index (LSI) calculation as the following equations:

$$LSI = pH - pHs$$

where pH is the actual pH and pHs is the saturation pH.

The pHs can be calculated from the relation, pHs = (9.3+A-B)-(C+D), where

$$A = \frac{\log[TDS]-1}{10},$$

$$B = -13.12 \times \log(^{o}C+273)+34.55,$$

$$C = \log[Ca^{+2} \text{ as } CaCO_3]-0.4,$$

$$D = \log[\text{alkalinity as } CaCO_3]$$

In our case for the real seawater from Red Sea: pH is 8.2, TDS is 41 g/L, Ca^{2+} is 0.255 g/L, HCO_3^- is 0.146 g/L, and water temperature on the surface of SiC-C (0.09y+0.09r) monolith is 38 ^{o}C (got from the IR image in Figure S15). As calculated based on Langelier Satuaration Index, pHs=7.8, and LSI=0.38, which means that water is supersaturated with respect to calcium carbonate ($CaCO_3$) and scale forming may occur.